

# The double-layer structure of overscreened surfaces by smeared-out ions

Derek Frydel\*

*Institute for Advanced Study, Shenzhen University, Shenzhen, Guangdong 518060, China*

(Dated: May 2, 2019)

Charge inversion occurring for smeared-out ions is accompanied by an oscillatory charge density profile, indicating a layering of an alternating charge. The layering effect, however, is not coextensive with charge inversion, and charge inversion accompanied by a monotonically decaying profile is possible. The present work focuses on the structure of a double-layer of overscreened charged surfaces by smeared-out charges and probes the link between the structure of a double-layer and the bulk properties of an electrolyte, with special view to the role of the Kirkwood crossover.

PACS numbers:

## I. INTRODUCTION

In our previous work we reported the possibility of charge inversion for ions with a smeared-out charge according to some distribution  $w(r) \neq \delta(r)$  [1, 2]. Because the phenomena was captured within the mean-field description, the underlying mechanism must not depend on correlations but is rather explained as weakening of interactions at short separations, especially repulsions between counterions near a charged surface due to gradual softening of a divergence in the Coulomb functional form. For point-ions, where  $w(r) = \delta(r)$  and with a divergence in pair interactions, the gain in free energy that leads to charge inversion is the outcome of partial ordering of counterions near a charged surface caused by strong correlations. Consequently, this correlation-based mechanism is not captured by the mean-field. Only an improved theory beyond the mean-field offers possibility for capturing this type of charge inversion [3–6].

In [1, 2] we focused primarily on the fact that a charge density and an electrostatic potential change sign, and we paid less attention to the far-field region, especially the presence in that region of oscillations. Our interest in the far-field region was recently reignited by a demonstration in [7] of the existence of the Kirkwood crossover – a point where a charge-charge correlation function changes from a monotonically to an oscillatory decaying profile – and a possible connection to our own results in [1]. As the onset of oscillations in a charge density profile naturally leads to charge inversion, we began to wonder about a possible role of the Kirkwood crossover in the mechanism of charge inversion. If indeed the occurrence of charge inversion is coextensive with an oscillatory decay, one may conclude that charge inversion is triggered by the Kirkwood crossover, and, therefore, is completely determined by the properties of a bulk electrolyte and independent of a charged surface. If, however, charge inversion may occur for monotonically decaying profile, then the picture is more subtle.

Consequently, the aim of the present work is to in-

vestigate charge inversion of smeared-out ions with special stress on the far-field behavior and the role of the Kirkwood crossover. Before embarking onto our specific project, however, we first want to review the Kirkwood crossover and provide justification for the expectation that a charge-charge correlation function and a charge density decay in the same fashion.

A characteristic of a fluid is a short-range translational order whereby correlations of a fluctuating variable decay exponentially as  $f(r)e^{-r/\xi}$ , where  $\xi$  implies the correlation length and  $f(r)$  is an algebraic function. Now, if we turn to an inhomogeneous fluid, we find that a density perturbation falls off exponentially as it merges with a uniform fluid, with the same exponential decay as found in correlations,  $g(r)e^{-r/\xi}$ , where the algebraic function  $g(r)$  depends on the geometry of a perturbation. This universality of an exponential decay is a consequence of the linear response theory wherein a perturbation is expressed as a superposition of fluctuations. Nonlinear effects of larger perturbations do not invalidate this interpretation as in the region where a perturbation merges with a bulk fluid a perturbation is once again small and the linear regime recovered.

A picture becomes more interesting if one considers dense fluids where the short-range translational order attains some degree of organization and the profile of a density-density correlation function develops a regular oscillating structure, albeit, that still decays exponentially. There are now two parameters describing a decay of correlations: a correlation length  $\xi$  and a wavelength  $\lambda$ . The point where oscillations first appear is known as the Fisher-Widom crossover [8, 9]. It is a crossover in a sense that it does not entail any macroscopic changes nor generate discontinuities in thermodynamic quantities. Non-analytic behavior, however, is observed in the correlation length  $\xi$ . Now, if we turn to inhomogeneous fluids, we find a similar structure in a density decay: an exponentially decaying oscillatory profile.

An analogous picture emerges for electrolytes, except now the relevant quantities are a charge density and a charge-charge correlation function. Here we also encounter a crossover from a monotonic to oscillatory decay that goes by the name of the Kirkwood crossover [10–12]. An interesting consequence of having oscillations in

---

\*Electronic address: dfrydel@gmail.com

a charge density around zero is repetitive charge inversion. This type of charge inversion depends only on the conditions of a bulk that control the quantities  $\xi$  and  $\lambda$  and cannot be induced by a surface charge or any specific feature of a perturbation.

A more "conventional" charge inversion involves monotonically decaying profiles and is the result of the renormalization of an effective charge. (The idea of an "effective charge" entails the idea of a "dressed surface", a surface comprised of a bare surface charge plus an adjacent layer of counterions that together reduce an absolute value of a bare charge). Being limited to the mean-field description, charge renormalization in this work is the result of nonlinear contributions of the mean-field theory in relation to its linear version, wherein a magnitude of a decaying profile is proportional to a surface charge. For the case of point-ions, the mean-field description does not predict the Kirkwood crossover, while the renormalized effective charge never changes sign, the effective charge saturates, and so the mean-field for point-charges does not predict charge inversion. Only a description beyond the mean-field level may capture charge inversion [2–5].

This work is organized as follows. In section II we formulate the mean-field theory for smeared-out ions. In section III we carry out the linear analysis to obtain the screening parameters and the location of the Kirkwood crossover for Gaussian distributed charges. In section IV we consider the full mean-field theory and focus on the renormalization of an effective surface charge for monotonically decaying profiles (prior to the Kirkwood crossover) and mark the region where charge inversion due to renormalization becomes possible. Finally, in section VI we conclude the work and make a number of connections to related systems, such as dumbbell ions and the primitive model.

## II. THE MEAN-FIELD DESCRIPTION

Within the standard representation, an electrolyte is made up of  $K$  different species of point-charges, and the Poisson equation is given by

$$\epsilon \nabla^2 \psi(\mathbf{r}) = - \sum_{i=1}^K q_i \rho_i(\mathbf{r}) \quad (1)$$

where  $\psi(\mathbf{r})$  is the electrostatic potential, and  $\rho_i(\mathbf{r})$  and  $q_i$  is a number density and a charge of a species  $i$ , respectively. If we move away from a point-charge description and consider ions represented as smeared-out charges within a spherically symmetrical distribution  $w_i(\mathbf{r} - \mathbf{r}')$ , normalized as  $\int d\mathbf{r}' w_i(\mathbf{r} - \mathbf{r}') = 1$ , then the Poisson equation is given by

$$\epsilon \nabla^2 \psi(\mathbf{r}) = - \sum_{i=1}^K q_i \int d\mathbf{r}' \rho_i(\mathbf{r}') w_i(\mathbf{r} - \mathbf{r}'), \quad (2)$$

and the case  $w_i(\mathbf{r} - \mathbf{r}') = \delta(\mathbf{r} - \mathbf{r}')$  recovers the Poisson equation for point charges. Note that a particle does not

need to be exactly at  $\mathbf{r}$  to contribute to a charge density at  $\mathbf{r}$ . Now all particles that are in sufficient vicinity of  $\mathbf{r}$ , that is within the distribution  $w(\mathbf{r} - \mathbf{r}')$ , contribute to a charge density, leading to a nonlocal term.

Similar consideration of nonlocality lead to the mean-field expression for a number density of smeared-out ions,

$$\rho_i(\mathbf{r}) = c_i e^{-\beta q_i \int d\mathbf{r}' \psi(\mathbf{r}') w_i(\mathbf{r} - \mathbf{r}')}, \quad (3)$$

where  $c_i$  is the bulk concentration of a species  $i$ . The nonlocality arises from the fact that now it is an entire distribution of an ionic charge that interacts with an average electrostatic potential  $\psi(\mathbf{r})$ , not just a particle center.

Inserting the mean-field number density into the Poisson equation of Eq. (2) yields a modified Poisson-Boltzmann equation for smeared-out ions,

$$\epsilon \nabla^2 \psi(\mathbf{r}) = - \sum_{i=1}^K c_i q_i \int d\mathbf{r}' w_i(\mathbf{r} - \mathbf{r}') e^{-\beta q_i \int d\mathbf{r}'' \psi(\mathbf{r}'') w_i(\mathbf{r}' - \mathbf{r}'')}. \quad (4)$$

Not surprisingly, correlational contributions diminish with increasing size of an ion. Consequently, the mean-field theory becomes virtually an exact model for representing ions with broad charge distributions. Our interest lies specifically in such a mean-field regime, where correlational contributions are minimal, so that any deviations from predictions of the point-charge model can be exclusively attributed to the finite size of ions.

## III. LINEAR ANALYSIS

As mentioned in the introduction, to describe an asymptotic decay within any theory – the screening parameter, the Kirkwood crossover, and the consequent wavelength of oscillations – the linear analysis is sufficient. Nonlinear contributions of the full mean-field do not alter this asymptotic region of interest and is considerably easier to handle.

Consequently, we proceed to linearize the modified PB equation of Eq. (4). Keeping only the linear terms, we get

$$\epsilon \nabla^2 \psi(\mathbf{r}) = \beta \sum_{i=1}^K c_i q_i \int d\mathbf{r}' \psi(\mathbf{r}') \int d\mathbf{r}'' w_i(\mathbf{r} - \mathbf{r}'') w_i(\mathbf{r}' - \mathbf{r}''). \quad (5)$$

For a symmetric monovalent electrolyte, where the net charge of an ion is  $q = \pm e$  ( $e$  is the fundamental charge), and the distributions are  $w_+(\mathbf{r} - \mathbf{r}') = w(\mathbf{r} - \mathbf{r}')$  and  $w_-(\mathbf{r} - \mathbf{r}') = -w(\mathbf{r} - \mathbf{r}')$ , the above equation further simplifies to

$$\epsilon \nabla^2 \psi(\mathbf{r}) = 2\beta c_s e^2 \int d\mathbf{r}' \psi(\mathbf{r}') \int d\mathbf{r}'' w(\mathbf{r} - \mathbf{r}'') w(\mathbf{r}'' - \mathbf{r}'). \quad (6)$$

To generate a nonuniform system, we perturb the uniform system by fixing a single ion at the origin, then obtain an electrostatic potential from the linear mean-field

theory,

$$\epsilon \nabla^2 \psi(r) = 2\beta e^2 c_s \int d\mathbf{r}' \psi(r') \int d\mathbf{r}'' w(\mathbf{r} - \mathbf{r}'') w(\mathbf{r}'' - \mathbf{r}') - ew(r). \quad (7)$$

Note that a fixed particle is taken to be positive. Fourier transforming the above equation yields

$$-\epsilon k^2 \psi(k) = 2\beta e^2 c_s \psi(k) w^2(k) - ew(k), \quad (8)$$

and the potential in the Fourier space is

$$\psi(k) = \frac{ew(k)}{\epsilon k^2 + 2\beta e^2 c_s w^2(k)}. \quad (9)$$

At this point we introduce more convenient reduced units,

$$\phi(k) = \frac{4\pi \lambda_B w(k)}{k^2 + \kappa_D^2 w^2(k)} \quad (10)$$

where  $\phi = \beta e \psi$ ,  $\lambda_B = \beta e^2 / (4\pi \epsilon)$  is the Bjerrum length, and  $\kappa_D^2 = 8\pi c_s \lambda_B$  is the Debye screening parameter. The electrostatic potential in real space is then obtained from inverse Fourier transform,

$$\phi(r) = \frac{2\lambda_B}{\pi} \int_0^\infty dk \frac{k^2 w(k)}{k^2 + \kappa_D^2 w^2(k)} \frac{\sin kr}{kr}. \quad (11)$$

For the case of point charges  $w(k) = 1$  and the above integral evaluates to a familiar screened potential  $\phi(r) = \lambda_B e^{-\kappa_D r} r^{-1}$ .

For particles with an arbitrary distribution  $w(r)$ , the integral in Eq. (11) can be conveniently handled using the residue theorem. To adopt the method to the present problem, we alter the limits of the integration as

$$\phi(r) = \frac{\lambda_B}{\pi i} \int_{-\infty}^\infty dk \frac{k w(k)}{k^2 + \kappa_D^2 w^2(k)} \frac{e^{ikr}}{r}. \quad (12)$$

which is allowed as long as  $w(k)$  is an even function, in which case the imaginary part cancels out. The need to alter the integration limits will become clear as we outline the details of the method.

In complex analysis the value of an integral along a closed curve  $C$  can be expressed as a sum of residues inside the region enclosed by  $C$ ,

$$\frac{1}{2\pi i} \oint_C dk f(k) = \sum_n \text{Res}(f, k_n). \quad (13)$$

In this case  $k$  is a complex variable, and  $\text{Res}(f, k_n)$  is a residue of  $f(k)$  at a pole  $k_n$ . A value of a residue corresponds to a coefficient  $a_{-1}$  in the expansion

$$f(k) = \sum_{m=-m_0}^\infty a_m (k - k_n)^m \quad (14)$$

carried out in the neighborhood of a pole  $k_n$ . A pole is said to be simple if  $m_0 = 1$ .

In order to apply Eq. (13) in evaluating the integral in Eq. (12), the curve  $C$  should incorporate the real axis, while the integral along the remaining curve (let's say a half circle with radius  $R \rightarrow \infty$ ) should evaluate to zero. If satisfied, then a potential can be represented as

$$\phi(r) = \frac{\lambda_B}{2\pi i} \oint_C dk f(k) = \lambda_B \sum_n \text{Res}(f, k_n), \quad (15)$$

with the integrand  $f(k)$  given by

$$f(k) = \frac{2k w(k)}{k^2 + \kappa_D^2 w^2(k)} \frac{e^{ikr}}{r}. \quad (16)$$

Poles, being singularities of the complex plane, correspond to zeros of the denominator of  $f(k)$ ,

$$k_n^2 + \kappa_D^2 w^2(k_n) = 0. \quad (17)$$

If poles enclosed by  $C$  are simple, and representing  $f(k)$  as a quotient of two functions  $g(k)/h(k)$ , the residues are given by

$$\text{Res}(f, k_n) = \frac{g(k_n)}{h'(k_n)}. \quad (18)$$

Together with Eq. (12) and Eq. (13), an electrostatic potential is then given by

$$\phi(r) = \lambda_B \sum_n \frac{e^{ik_n r}}{r} \frac{k_n w(k_n)}{k_n + \kappa_D^2 w(k_n) w'(k_n)}. \quad (19)$$

It is now clear that the poles, expressed as,

$$k_n = i\kappa_n + \omega_n, \quad (20)$$

characterize a screening parameter  $\kappa_n$  and a wavenumber  $\omega_n$  of each term in Eq. (19). Since the linear theory accurately describes only a far-field region, we are only interested in the dominant term, that is, the pole with the smallest  $\kappa_n$ .

Note that only a strictly imaginary  $k_n$  yields a monotonically decaying function. On the other hand, a strictly real  $k_n$  yields a solid like structure with a long-range translational order. A fully complex pole determines an oscillating exponentially decaying profile.

#### A. $w(r)$ as a Gaussian distributed function

As a specific case, we consider ions with a Gaussian distributed charge,

$$w(r) = \frac{e^{-r^2/2\sigma^2}}{(2\pi\sigma^2)^{3/2}}, \quad (21)$$

whose Fourier transform is

$$w(k) = e^{-k^2\sigma^2/2}, \quad (22)$$

and an electrostatic potential within a linearized mean-field theory is given by

$$\phi(r) = \frac{\lambda_B}{\pi i} \int_{-\infty}^{\infty} dk \frac{k e^{-k^2 \sigma^2/2}}{k^2 + \kappa_D^2 e^{-k^2 \sigma^2}} \frac{e^{ikr}}{r}, \quad (23)$$

then the poles are determined from the relation

$$k_n^2 + \kappa_D^2 e^{-k_n^2 \sigma^2} = 0, \quad (24)$$

or, after rearrangement,

$$-\kappa_D^2 \sigma^2 = k_n^2 \sigma^2 e^{k_n^2 \sigma^2}, \quad (25)$$

where  $-\kappa_D^2 \sigma^2$  appears as a function of  $k_n^2 \sigma^2$ . But being interested in  $k_n^2 \sigma^2$  as a function of  $-\kappa_D^2 \sigma^2$ , we look for an inverted relation that, in fact, is provided by the Lambert multivalued function

$$W_n(-\kappa_D^2 \sigma^2) = k_n^2 \sigma^2, \quad (26)$$

where  $n$  denotes a particular branch, with  $n = 0$  being the principal branch. The poles are now expressed as

$$k_n \sigma = i \sqrt{-W_n(-\kappa_D^2 \sigma^2)}, \quad (27)$$

and the electrostatic potential within the linear mean-field theory is

$$\phi(r) = \sum_{n=-\infty}^{\infty} \frac{\lambda_B e^{ik_n r}}{r} \frac{e^{-k_n^2 \sigma^2/2}}{1 - k_n^2 \sigma^2}. \quad (28)$$

In Fig. (1) we plot the screening parameters  $\kappa_n$ , given by

$$\kappa_n = \text{Re} \left[ \sqrt{-W_n(-\kappa_D^2 \sigma^2)} \right], \quad (29)$$

for a number of initial branches as a function of  $\kappa_D \sigma$ . First thing to note is the apparent non-analyticity of  $\kappa_0$  and  $\kappa_{-1}$ , the two lowest branches that determine the far-field decay, through the point  $\kappa_D \sigma = e^{-1/2}$ , where the dominant screening parameter  $\kappa_0$  switches from an increasing to a decreasing function of  $\kappa_D \sigma$ , indicating the growth of the correlation length with density. Non-analyticity signals the Kirkwood crossover, and the two branches  $n = 0, -1$  determining the far-field asymptotics develop oscillations for  $\kappa_D \sigma > e^{-1/2}$ .

In Fig. (2) we plot the wavelengths  $\lambda_n = 2\pi/\omega_n$  where

$$\omega_n = \text{Im} \left[ \sqrt{-W_n(-\kappa_D^2 \sigma^2)} \right], \quad (30)$$

for a number of initial branches. At the Kirkwood crossover, as  $\kappa_D \sigma$  approaches  $e^{-1/2}$  from above,  $\lambda_0$  (and  $\lambda_{-1}$ ) diverges, indicating the absence of oscillations for  $\kappa_D \sigma < e^{-1/2}$ . All the remaining  $\lambda_n$  diverge only as  $\kappa_D \sigma \rightarrow 0$ , as these terms are always oscillating.

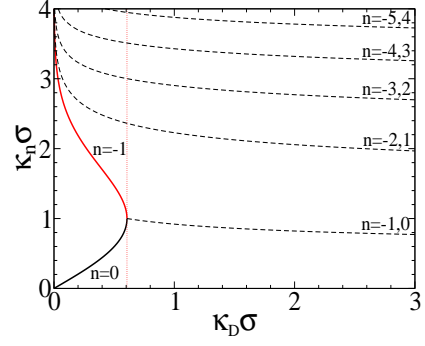


FIG. 1: Screening parameters  $\kappa_n$  for a number of initial branches for Gaussian distributed ion. The solid lines indicate the screening of monotonic and the dashed lines of oscillatory terms. For  $\kappa_D \sigma > e^{-1/2}$  all terms have oscillations and the point  $\kappa_D \sigma = e^{-1/2}$  (a vertical dotted line) is referred to as the Kirkwood crossover.

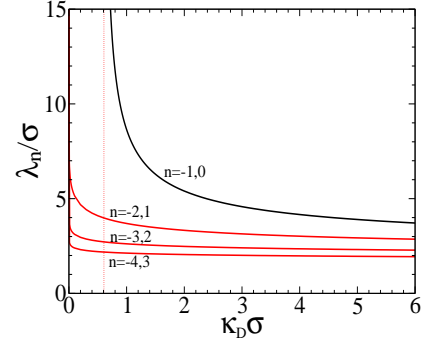


FIG. 2: Wavelengths  $\lambda_n = \frac{2\pi}{\omega_n}$  for a number of initial branches as a function of  $\kappa_D \sigma$  for initial branches.  $\lambda_0$  (which is equivalent with  $\lambda_{-1}$ ) diverges at the Kirkwood crossover and the remaining wavelengths diverge as  $\kappa_D \sigma \rightarrow 0$ .

The crucial result of this section is the location of the Kirkwood crossover at  $\kappa_D \sigma = e^{-1/2}$  and the precise determination of parameters governing the far-field decay,  $\kappa_0$  and  $\lambda_0$ . The Kirkwood crossover splits an electrolyte into two domains. Beyond the crossover the far-field decay of a charge density profile changes from monotonic to oscillatory. The onset of oscillations in a charge density necessarily implies a repetitive charge inversion. Such charge inversion is fundamentally different from a more conventional charge inversion that results from renormalization of an effective charge, firstly, because of its oscillating nature, and, secondly, because it depends on bulk properties alone. In contrast, conventional charge inversion happens for monotonically decaying profiles (prior to the Kirkwood crossover) and is triggered by strong correlations between counterions near a charged surface, therefore, the magnitude of a surface charge plays an important role [3–5].

In Fig. (3) we plot charge density profiles generated by a fixed ion (but excluding a charge density of that ion)

and obtained from the Fourier transform of

$$\rho_c(k) = -2c_s w^2(k) \phi(k) \quad (31)$$

which in real space yields, using the residue theorem,

$$\rho_c(r) = -\frac{\kappa_D^2}{4\pi} \sum_{n=-\infty}^{\infty} \frac{e^{ik_n r}}{r} \frac{e^{-3k_n^2 \sigma^2/2}}{1 - k_n^2 \sigma^2}. \quad (32)$$

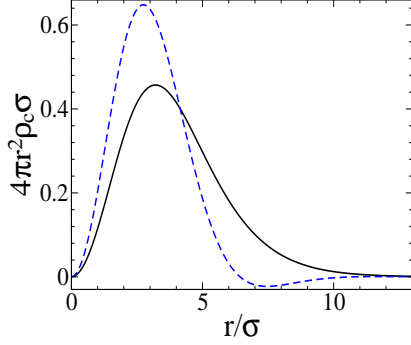


FIG. 3: Charge density profiles,  $4\pi r^2 \rho_c(r)$ , around a fixed particle for  $\kappa_D \sigma = 0.6$  (before the crossover, solid line) and  $\kappa_D \sigma = 1$  (after the crossover, dashed line). The Kirkwood crossover is at  $\kappa_D \sigma = e^{-1/2} \approx 0.607$

#### IV. THE FULL MEAN-FIELD

Having determined the screening parameters and the location of the Kirkwood crossover from linear analysis, we next turn to a full mean-field description. Our interest lies primarily in the region before the Kirkwood crossover,  $\kappa_D \sigma < e^{-1/2}$ , where we investigate the nonlinear renormalization of an effective charge of monotonically decaying profiles, and we focus on the possibility of charge inversion.

Before investigating the full mean-field theory of smeared-out ions, we first review the results for point-ions,  $w(r) \rightarrow \delta(r)$ , whose full mean-field description corresponds to the standard Poisson-Boltzmann equation, and which, for the wall model, is given by

$$\phi''(x) = \kappa_D^2 \sinh \phi(x) - 4\pi \lambda_B \sigma_c \delta(x). \quad (33)$$

After adapting the Debye screening length  $\kappa_D^{-1}$  as a length scale (so that the dimensionless length is  $y = \kappa_D x$ ) the above equation becomes

$$\phi''(y) = \sinh \phi(y) - \left( \frac{4\pi \lambda_B \sigma_c}{\kappa_D} \right) \delta(y). \quad (34)$$

It now becomes clear that the functional form of  $\phi(y)$  depends on a single parameter  $4\pi \lambda_B \sigma_c \kappa_D^{-1}$ . Within the linear regime given by

$$\phi''_{\text{lin}}(y) = \phi_{\text{lin}}(y) - \left( \frac{4\pi \lambda_B \sigma_c}{\kappa_D} \right) \delta(y), \quad (35)$$

the solution is

$$\phi_{\text{lin}}(x) = \left( \frac{4\pi \lambda_B \sigma_c}{\kappa_D} \right) e^{-\kappa_D x}. \quad (36)$$

The nonlinear contributions do not renormalize the screening parameter, and the only parameter that is modified is the magnitude of the far-field decay, or, as mentioned before, the "effective" surface charge  $\sigma_c^{\text{eff}}$ , which is obtained by fitting the far-field potential to the functional form

$$\phi(x) \approx \left( \frac{4\pi \lambda_B \sigma_c^{\text{eff}}}{\kappa_D} \right) e^{-\kappa_D x}, \quad (37)$$

or more simply

$$\phi(x) \approx A e^{-\kappa_D x}, \quad (38)$$

where  $A$  is a single fitting parameter. Because Eq. (43) for point-ions admits an analytical solution,

$$\phi(y) = 2 \log \left[ \frac{4 + A e^{-y}}{4 - A e^{-y}} \right], \quad (39)$$

which far away from a charged surface reduces to

$$\phi(x) = A e^{-\kappa_D x} + O(e^{-3\kappa_D x}), \quad (40)$$

the expression for  $A$ , by considering the following boundary conditions at a charged surface

$$\phi'(0) = -4\pi \lambda_B \sigma_c, \quad (41)$$

is given by

$$A = 4 \left( \sqrt{1 + \left( \frac{2\kappa_D}{4\pi \lambda_B \sigma_c} \right)^2} - \frac{2\kappa_D}{4\pi \lambda_B \sigma_c} \right). \quad (42)$$

In Fig. (4) we plot the coefficient  $A = 4\pi \lambda_B \sigma_c^{\text{eff}} \kappa_D^{-1}$  as a function of  $4\pi \lambda_B \sigma_c \kappa_D^{-1}$ . The linear regime (indicated by a dotted line) breaks down already around  $4\pi \lambda_B \sigma_c \kappa_D^{-1} \approx 1$  where the nonlinear contributions reduce the effective surface charge, eventually leading to saturation of  $A$  (or  $\sigma_c^{\text{eff}}$ ). Saturation implies that a charged surface no longer releases counterions into a solution but keeps them as part of a "dressed surface". Saturation is then the strongest effect of the nonlinear contributions. For point-ions charge inversion becomes possible within an improved theoretical description beyond the mean-field [3–5].

We next turn to smeared-out ions. The modified Poisson-Boltzmann equation for the wall geometry is

$$\begin{aligned} \phi''(y) = & (\kappa_D \sigma)^2 \int d\mathbf{y}' w(\mathbf{y}, \mathbf{y}') \sinh \left[ \int d\mathbf{y}'' w(\mathbf{y}', \mathbf{y}'') \phi(y'') \right] \\ & - (4\pi \lambda_B \sigma_c \sigma) \delta(y) \end{aligned} \quad (43)$$

where the unit of length is taken to be the size of an ion,  $\sigma$  (now a reduced length is defined as  $y = x/\sigma$ ). The

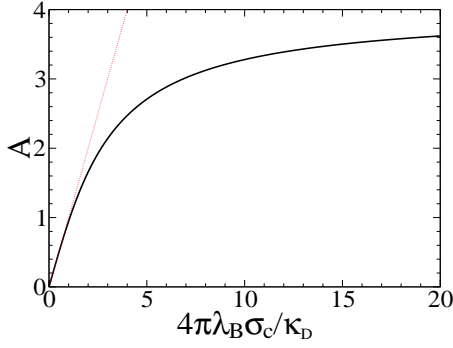


FIG. 4: The coefficient  $A = 4\pi\lambda_B\sigma_c^{\text{eff}}\kappa_D^{-1}$  as a function of  $4\pi\lambda_B\sigma_c/\kappa_D$  obtained by fitting the far-field potential to a functional form  $Ae^{-\kappa_D x}$ . The dotted line corresponds to the coefficient  $A$  within a linear solution in Eq. (36),  $A_{\text{lin}} = 4\pi\lambda_B\sigma_c/\kappa_D$ .

functional form of  $\phi(y)$  now depends on two parameters,  $\kappa_D\sigma$  and  $4\pi\lambda_B\sigma_c\sigma$ , resulting in a more complicated solution than that for point-ions. This additional degree of freedom provides an alternative route to charge inversion without contributions from correlations.

In Fig. (5) we plot the coefficient  $A$  as a function of  $4\pi\lambda_B\sigma_c\sigma$  for  $\kappa_D\sigma = 0.35 < e^{-1/2}$ , obtained by fitting a potential at the far-field to the functional form  $Ae^{-\kappa_0 x}$ , where

$$\kappa_0\sigma = \text{Re} \left[ \sqrt{-W_0(-\kappa_D^2\sigma^2)} \right]. \quad (44)$$

As compared with a similar plot for point-ions in Fig. (4), the nonlinear renormalization of  $A$  is considerably stronger. After an incipient growth  $A$  reaches a maximum at  $4\pi\lambda_B\sigma_c\sigma \approx 2.3$  then at  $4\pi\lambda_B\sigma_c\sigma \approx 9.1$  it changes sign, indicating the onset of charge inversion. The inverted effective charge, however, does not increase indefinitely, and  $A$  attains a minimum at  $4\pi\lambda_B\sigma_c\sigma \approx 27.7$  after which it starts to approach zero for the second time, leading eventually to a subsequent charge inversion. It is expected that  $A$  is an oscillating function of  $4\pi\lambda_B\sigma_c\sigma$ , so that by increasing  $4\pi\lambda_B\sigma_c\sigma$  indefinitely one can generate an arbitrary number of alternating layers of charge.

In Fig. (6) we plot a similar plot but for  $\kappa_D\sigma = 0.47$ . As might be expected, the effect of nonlinear contributions is larger but general features remain intact.

We note that for point-ions the coefficient  $A$  is defined as  $A = 4\pi\lambda_B\sigma_c^{\text{eff}}\kappa_D^{-1}$ , while for smeared-out ions it is

$$A = 4\pi\lambda_B\sigma_c^{\text{eff}}\sigma a(\kappa_D\sigma), \quad (45)$$

where  $a$  is a function of  $\kappa_D\sigma$  given by a linear solution of a wall model, and for the two cases considered above,  $a(0.33) = 12.5$  and  $a(0.47) = 20.3$ .  $\sigma_c^{\text{eff}}$ , on the other hand, depends on a bare surface charge but not  $\kappa_D$ , and for fixed  $\kappa_D\sigma$ ,  $A$  can be talked about as an effective surface charge.

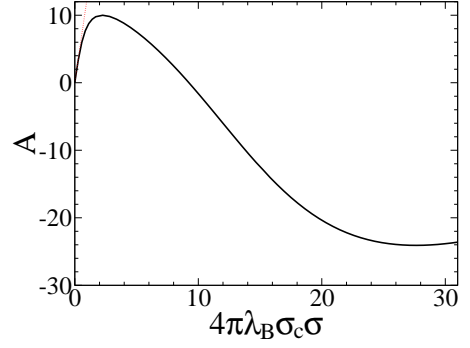


FIG. 5: Coefficient  $A$  (determined by matching the far-field behavior to the functional form  $Ae^{-\kappa_0 x}$ ) as a function of a bare surface charge. The plot is for  $\kappa_D\sigma = 0.33$ , before the Kirkwood crossover at  $\kappa_D\sigma = e^{-1/2} \approx 0.607$ , and the system is a wall model.

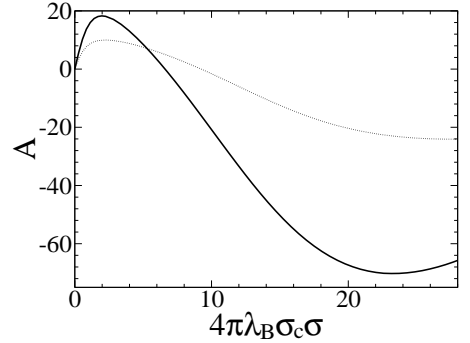


FIG. 6: Coefficient  $A$  (determined by matching the far-field behavior to the functional form  $Ae^{-\kappa_0 x}$ ) as a function of a bare surface charge. The plot is for  $\kappa_D\sigma = 0.47$ , before the Kirkwood crossover at  $\kappa_D\sigma = e^{-1/2} \approx 0.607$  and the system is a wall model. The dashed line is for comparison and corresponds to  $\kappa_D\sigma = 0.33$  of Fig. (5).

Comparing two curves in Fig. (6) we see that the point where charge inversion first occurs shifts to different values of  $4\pi\lambda_B\sigma_c\sigma$ . In Fig. (7) we plot a large number of such points in the  $(\kappa_D\sigma, 4\pi\lambda_B\sigma_c\sigma)$  plane, thereby, demarcate the region where charge inversion becomes possible. The region *II* represents the region beyond the Kirkwood crossover. Here charge inversion occurs by virtue of an oscillating profile. The region *I* represents parameters, prior to the Kirkwood crossover, where charge inversion occurs by virtue of nonlinear renormalization of an effective charge.  $4\pi\lambda_B\sigma_c\sigma \approx 3$  can be considered as a threshold for charge inversion due to charge renormalization, since for  $4\pi\lambda_B\sigma_c\sigma \lesssim 3$  this type of charge inversion becomes impossible due to too weak nonlinear contributions.

To further characterize charge inversion, in Fig. (8) we plot the shortest distance from a wall at which a potential changes sign,  $\phi(r_c) = 0$ . At the onset of charge inversion  $r_c \rightarrow \infty$ , as  $\kappa_D\sigma$  approaches the point of inversion from

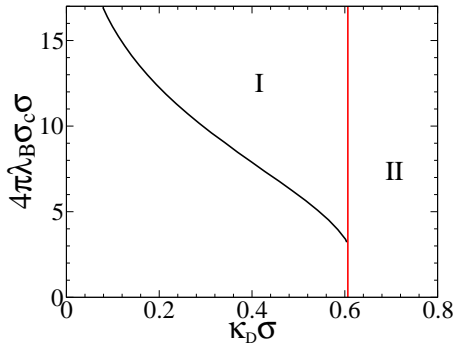


FIG. 7: A diagram demarcating regions where charge inversion occurs. The region *II* corresponds to a region beyond the Kirkwood crossover, where charge inversion occurs by virtue of an oscillating charge density around zero. The region *I* corresponds to charge inversion, before the Kirkwood crossover, due to nonlinear renormalization of the coefficient  $A$ .

above. Within the linear theory, divergence coincides with the Kirkwood crossover. On the other hand, the nonlinear contributions of the full mean-field theory push the divergence beyond the Kirkwood crossover. This divergence happens to be steeper than that at the Kirkwood crossover.

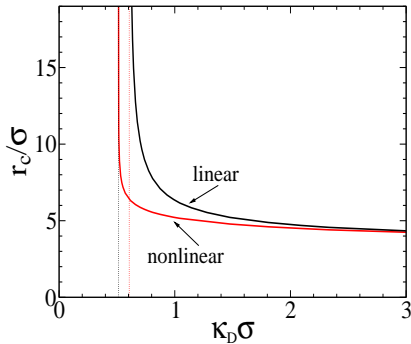


FIG. 8: The shortest distance from a wall at which a potential becomes zero,  $\phi(r_c) = 0$ , as a function of  $\kappa_D\sigma$  for a charged wall model, for a linear and full mean-field theory. The results are for  $4\pi\lambda_B\sigma_c\sigma \approx 5.65$ .

Finally, in Fig. (9) we plot charge density profiles of a wall model for  $4\pi\lambda_B\sigma_c\sigma \approx 14$  for three different values of  $\kappa_D\sigma$ : 0.1, 0.57, and 3.3, each lying in a different region of Fig. (7). The curvature for  $\kappa_D\sigma = 0.57 < e^{-1/2}$  exhibits charge inversion without oscillations. For  $\kappa_D\sigma = 3.3 > e^{-1/2}$ , which lies beyond the Kirkwood crossover, oscillations are clearly visible.

## V. DUMBBELL IONS

To broaden the perspectives we consider another model of extended ions, the dumbbells, ions made up of two

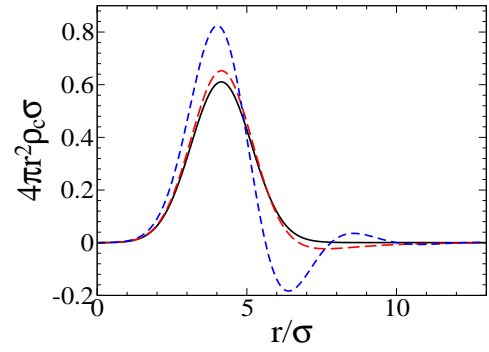


FIG. 9: Charge density profile for a wall model obtained from a full mean-field theory. The results are for  $4\pi\lambda_B\sigma_c\sigma = 14$  and for three different values of  $\kappa_D\sigma$ : 0.1, 0.57, and 3.3. See Fig. (7) to locate these points in the  $(\kappa_D\sigma, 4\pi\lambda_B\sigma_c\sigma)$  plane.

point charges  $q$  separated by a distance  $\sigma$ , which is an example of non-spherical distribution  $w(\mathbf{r} - \mathbf{r}', \mathbf{n})$ , where  $\mathbf{n}$  is the unit vector and represents orientation of a dumbbell.

The mean-field treatment of dumbbell ions shows that two same charged plates attract one another when a single dumbbell counterion forms a bridge between two same charged surfaces [2, 13–16]. As the phenomena of attraction between same charged surfaces is related to charge inversion, we should expect that dumbbell ions under favorable conditions can also produce charge inversion. However, for dumbbells we have an additional parameter of orientation, and so dumbbells with parallel orientation to a charged surface behave as point-ions within the mean-field description. Only configurations that deviate from parallel orientation yield results different from those of a point-charge model. A useful quantity in connection to this is the orientational parameter,

$$S = \frac{3\langle \cos^2 \theta \rangle - 1}{2}, \quad (46)$$

used for liquid crystals. For perfect alignment  $S = 1$ , for random distribution  $S = 0$ , and  $S < 0$  indicates the preference for parallel orientation with the lowest value being  $S = -1/2$ .

The modified PB equation for a dumbbell symmetric electrolyte, for a planar wall geometry, is

$$\phi''(x) = \frac{\kappa_D^2}{2\sigma} \int_{-\sigma}^{\sigma} dx' \sin \left[ \frac{\phi(x) + \phi(x+x')}{2} \right], \quad (47)$$

where the total charge  $e$  is equally divided between two ends, that is, each end has a charge of  $e/2$ .

In Fig. (10)(a) we plot the electrostatic potential near a planar charged wall for a dumbbell electrolyte. We compare two possible orientation rules: in one case the planar wall restricts position of ions but not their orientations, in another case the same wall restricts also orientations when ion endpoints are not allowed to cross



the wall, enforcing ions near a wall into parallel orientation. In Fig. (10) (b) we plot the orientational parameter  $S$  of counterions near a charged wall for the two cases. It is clear that by permitting free orientation, ions tend to align themselves perpendicular to a wall, thereby, the effect of charge extension is maximized. This is reflected in the plot of electrostatic potential, where charge inversion for the case of free ions is considerably more pronounced.

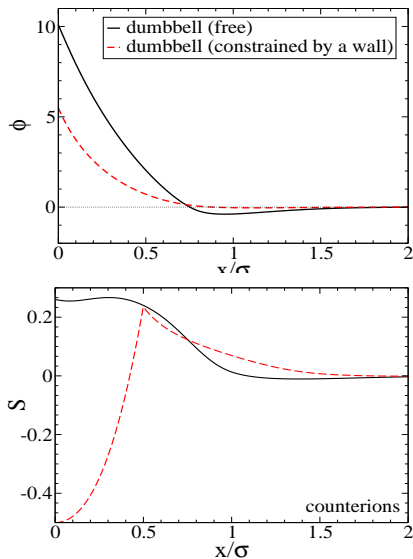


FIG. 10: Electrostatic potential and orientation parameter  $S$  as a function of a distance from a wall. The physical parameters of the system are:  $\sigma = 0.8$  nm,  $\lambda_B = 0.72$  nm,  $\sigma_c = 0.4$  Cm $^{-2}$ ,  $c_s = 1$  M. And the reduced relevant parameters are  $\kappa_D \sigma = 2.64$  and  $4\pi\lambda_B \sigma_c \sigma = 18.07$ .

## VI. CONCLUSION

We have described charge inversion for smeared-out ions as falling into two categories, depending where a

bulk electrolyte of a reservoir is with respect to the Kirkwood crossover. For a bulk prior to the Kirkwood crossover, charge inversion occurs by virtue of nonlinear renormalization of an effective charge and a charge density profile decays monotonically. For a bulk beyond the Kirkwood crossover, a charge density develops oscillations, producing charge layering. This type of charge inversion is captured within a linear regime of the mean-field. The link between bulk properties of an electrolyte and an interfacial structure of a charge could provide, at least in principle, the means for determination of the Kirkwood crossover from analyzing the structure of a double-layer.

We have, in addition, considered briefly dumbbell ions as an example of ions with non-spherically distributed charge. In this case the size of an ion alone does not determine the degree of nonlocality of an ion charge, which in addition depends on orientation. (The nonlocal effect is maximized by orientations perpendicular to a surface). The dumbbell ions are found to produce charge inversion, confirming the view that charge inversion is a general feature of ions with nonlocal charge distribution.

The role of the Kirkwood crossover should not be limited to smeared-out ions. A different example would be electrolytes based on primitive models, where the onset of oscillations arises as a problem of packing. We should expect that these systems too produce oscillating charge density profiles beyond the Kirkwood crossover. A look into available literature reveals a number of studies having reported such an oscillating behavior [17], without an explicit link to the Kirkwood crossover. A more systematic study of charge density profiles for a number of different primitive models can be found in [18].

## Acknowledgments

This research was supported by the Chinese National Science Foundation, the grant number 11574198. Some computations were done using machines of the Laboratoire de Physico-Chimie Théorique, ESPCI.

- 
- [1] D. Frydel and Y. Levin, *J. Chem. Phys.* **138**, 174901 (2013).
  - [2] D. Frydel, *Adv. Chem. Phys.* **160**, (2016).
  - [3] G. Téllez, (2005), *J. Stat. Phys.* **122**, 787 (2005).
  - [4] G. Téllez, *Europhys. Lett.*, **76**, 1186 (2006).
  - [5] L. Šamaj, *J. Stat. Phys.* **124**, 1179 (2006).
  - [6] D. Frydel and M. Ma, *Phys. Rev. E* **93**, 062112 (2016).
  - [7] A. Nikoubashman, J.-P. Hansen, and G. Kahl, *J. Chem. Phys.* **137**, 094905 (2012).
  - [8] R. Evans, R. J. F. Leote de Carvalho, J.-R. Henderson, D.C. Hoyle, *J. Chem. Phys.* **100**, 591 (1994).
  - [9] A. J. Archer and R. Evans, *Phys. Rev. E* **64**, 041501 (2001).
  - [10] J. G. Kirkwood, *Chem. Rev.* **19**, 275 (1936).
  - [11] R. J. F. Leote de Carvalho and R. Evans, *Mol. Phys.* **83**, 619 (1994).
  - [12] J. Ulander and R. Kjellander, *J. Chem. Phys.* **109**, 9508 (1998).
  - [13] Y. W. Kim, J. Yi, and P. A. Pincus, **101**, 208305 (2008).
  - [14] J. Urbanija, K. Bohinc, A. Bellen, S. Maset, A. Iglič, *J. Chem. Phys.* **129**, 105101 (2008).
  - [15] V. B. Teifa, K. Bohinc, *Prog. Biophys. Mol. Biol.* **105**, 208 (2011).
  - [16] K. Bohinc, *Prog. Biophys. Kem. Ind.* **63**, 93 (2014).
  - [17] Y.-X. Yua, J. Wu, G.-H. Gao, *J. Chem. Phys.* **120**, 7223 (2004).
  - [18] M. Ding, Y. Liang, B. Lu, and X. Xing, <https://arxiv.org/pdf/1502.06687.pdf>.